

Research Article www.acsami.org

# Influence of the Exclusion-Enrichment Effect on Ion Transport in Two-Dimensional Molybdenum Disulfide Membranes

Xin Tong, Su Liu,\* Yangying Zhao, Yongsheng Chen, and John Crittenden



Cite This: ACS Appl. Mater. Interfaces 2021, 13, 26904–26914



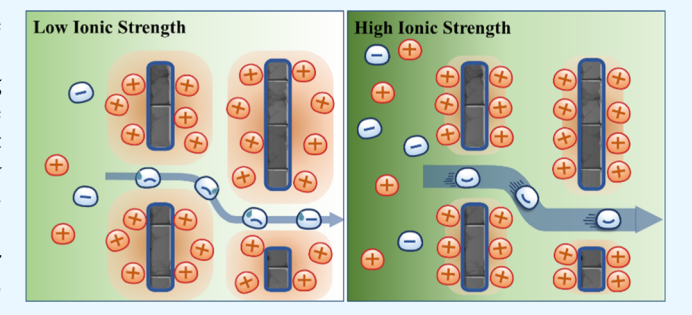
**ACCESS** I

III Metrics & More

Article Recommendations

Supporting Information

ABSTRACT: Two-dimensional (2D) nanosheet membranes have been widely studied for water and wastewater treatment. However, mass transport inside 2D nanosheet membranes is far from being fully understood, and suitable applications of these membranes are yet to be identified. In this study, we investigate ion transport inside a 2D molybdenum disulfide (MoS<sub>2</sub>) membrane by combining experimental results with numerical modeling. Specifically, we analyze the influence of the electrical double layer (EDL) extension on ion diffusion in the MoS<sub>2</sub> membrane, and a parameter called the exclusion-enrichment coefficient  $(\beta)$  is introduced to quantify how the electrostatic interaction between the coions and



the EDL can affect the ion diffusion. Using the model developed in this study, the  $\beta$  values under different experimental conditions (feed solution concentration and applied hydraulic pressure) are calculated. The results show that coion diffusion inside the membrane can be retarded since  $\beta$  is smaller than one. Furthermore, the underlying mechanism is explored by theoretically estimating the radial ion concentration and electrical potential distributions across the membrane nanochannel. In addition, we find that convective mass transport can weaken the exclusion-enrichment effect by increasing  $\beta$ . Based on the results in this study, the potential applications and feasible membrane design strategies of 2D nanosheet membranes are discussed.

KEYWORDS: 2D material, exclusion-enrichment effect, membrane separation, molybdenum disulfide, ion transport

# **■** INTRODUCTION

Water scarcity is recognized as one of the largest challenges in the 21st century. The development of robust and sustainable technologies to reclaim clean water from unconventional sources, such as seawater, brackish water, and wastewater, can largely alleviate global water scarcity. Membrane technologies can play an important role in water treatment, wastewater reclamation, and desalination.<sup>3,4</sup> Freshwater of superior quality can be produced from membrane-based treatment technologies; at the same time, membrane-based treatment technologies have a smaller footprint and higher energy efficiency than conventional water treatment technologies.5 For instance, state-of-theart thin-film composite (TFC) membranes are widely used for reverse osmosis seawater desalination and water reuse. 6 A nonporous polyamide active layer ensures that the TFC membrane can have high contaminant rejection, satisfactory water permeability, and a wide pH operation range (pH 2-11). However, the current design and fabrication of commercial membranes for water treatment largely depend on empirical approaches instead of molecular-level design, which hinders the further improvement of membrane separation performance.<sup>5,8</sup> Regarding TFC membranes, the inability to control their active layer structure during membrane synthesis results in a permeability-selectivity trade-off,9 which limits the achievable membrane selectivity and increases the cost of water treatment.

To overcome such limitations, novel materials and molecularlevel design approaches have been extensively studied to advance membrane technologies for water purification and desalination.

Exfoliated two-dimensional (2D) nanosheet membranes have demonstrated excellent separation performance as semipermeable membranes for water and wastewater treatment. 10 2D nanosheet membranes are commonly synthesized on the lab scale by either pressure-assisted filtration (including vacuum filtration)<sup>11,12</sup> or layer-by-layer (LbL) dip coating. <sup>13,14</sup> The synthesized membrane contains numerous interconnected nanochannels with sharp molecular cutoffs that can effectively reject solutes. 15 As the most widely studied 2D material for membrane fabrication, graphene oxide (GO) has been utilized to design a variety of membranes for solute retention by tuning its interlayer spacing.<sup>16</sup> Nevertheless, the hydration of hydrophilic functional groups at the edges of the GO nanosheets can cause swelling of the GO membrane in solutions, which impairs

Received: February 27, 2021 Accepted: May 21, 2021 Published: June 3, 2021





the solute retention performance and selectivity of the membrane.<sup>17</sup> To circumvent the issue that GO membranes face, other 2D nanosheets, including hexagonal boron nitride (h-BN), 18 transition metal dichalcogenides (TMDs), 19 and transition metal carbides (MXene). To have also been utilized for 2D nanosheet membrane fabrication. For example, laminate membranes fabricated using molybdenum disulfide ( $MoS_2$ ), the most extensively studied TMD, are structurally more stable in water.21

The mechanisms responsible for the solute rejection of 2D nanosheet membranes have also been actively explored. An experimental investigation suggested that the GO membrane has a sharp molecular cutoff, and ions or molecules with a hydrated radius larger than 4.5 Å can be blocked by the membrane.<sup>22</sup> More subsequent studies confirmed that steric (size) exclusion is a dominant ion retention mechanism for 2D nanosheet membranes. 20,23,24 Thus, by tuning the interlayer spacing between adjacent 2D nanosheets, selective sieving of different ions and molecules can be achieved. 25,26 Furthermore, electrostatic exclusion was also demonstrated to play an important role during ion transport across 2D nanosheet membranes.<sup>21,24,27</sup> However, charge-regulated transport is far from being fully understood, and a satisfying theoretical framework to describe ion transport inside 2D nanosheet membranes is yet to be established.

Studies on mass transport in nanofluidic channels have indicated that the diffusion of ions and/or charged molecules is highly influenced by the extension of the electrical double layer (EDL). 28 The EDL causes specific charge (re) distribution at the interface of the channel surface and the solution so that the fixed charges on the channel surface can be compensated by the mobile counterions in the solution.<sup>29</sup> The thickness of the EDL depends on the solution ionic strength and can range from less than 1 nm to more than tens of nanometers. An electrostatic screening zone can be formed inside the EDL; inside the zone, an enrichment of counterions and exclusion of coions result due to electrostatic interactions, and this phenomenon is named the exclusion-enrichment effect. 30 Since the EDL represents a significant fraction of the total volume inside the nanochannel in many cases, the exclusion-enrichment effect can have an influence on the transport of ions and/or charged molecules. Moreover, when the thickness of the EDL becomes larger, which is referred to as the extension of the EDL, the exclusionenrichment effect can become stronger since more volume inside the nanochannel is occupied by the EDL. Specifically, for a charged nanochannel, counterions diffuse faster than coions; 30,31 for a single salt solution, the counterion diffusion rate equals that of the coions since electroneutrality needs to be fulfilled, which leads to retarded salt diffusion.

The 2D nanosheet membranes contain well-defined nanochannels with fixed charges that can influence the transport of charged species. However, the exclusion-enrichment effect inside 2D nanosheet membranes remains unexplored. In this study, we investigated ion transport across MoS2 membranes by combining experimental efforts with theoretical modeling. A numerical model was developed to describe ion transport inside the MoS<sub>2</sub> membrane. Specifically, we found that the exclusionenrichment effect induced by the extension of the EDL retarded the diffusion of ions inside the MoS<sub>2</sub> membranes. Furthermore, we explored the influence of convection (advection) on the exclusion-enrichment effect of the EDL; we found that when convective mass transport (induced by volumetric water flux) becomes more dominant, the influence of EDL extension on

diffusive mass transport becomes weaker. Based on the results of this study, we discussed the potential applications of MoS<sub>2</sub> membranes and other 2D nanosheet membranes in the realm of water and wastewater treatment. Future design strategies of 2D nanosheet membranes are also discussed.

#### MATERIALS AND METHODS

Synthesis of Molybdenum Disulfide Nanosheets and Membranes. MoS<sub>2</sub> nanosheets were synthesized using a liquidphase exfoliation method. 32,33 First, 500 mg of bulk MoS<sub>2</sub> powder (Millipore Sigma, Burlington, MA, USA) was dispersed in 50 mL of isopropyl alcohol. The prepared dispersion was then sonicated for 48 h. The resulting dispersion was centrifuged (Eppendorf 5430R, Hamburg, Germany) at 5000 rpm (G = 2600) five times, and the obtained supernatant was collected and diluted with DI water after each centrifugation step. After the centrifugation process was completed, the resulting suspension was diluted to a concentration of 0.5 mg/mL and stored for further characterization. Vacuum filtration was used to fabricate the MoS<sub>2</sub> laminate membrane.<sup>34</sup> A polyvinylidene fluoride (PVDF) membrane (Millipore Sigma, Burlington, MA, USA) with a diameter of 47 mm and a pore size of 0.22  $\mu$ m was used as the substrate for fabricating the  $MoS_2$  membranes. The thickness of the  $MoS_2$ membrane was controlled by the volume of the dispersion. The fabricated MoS<sub>2</sub> membrane was stored in DI water for further

Characterization of Molybdenum Disulfide Nanosheets and **Membranes.** The hydrodynamic size distribution of the as-prepared MoS<sub>2</sub> nanosheets was characterized using a Nano-ZS (ZEN 3600) Malvern Zetasizer (Malvern Instruments, Inc., Worcestershire, UK). Before size distribution characterization, the as-prepared MoS<sub>2</sub> suspension (0.5 mg/mL) was diluted 100 times. The zeta potential of the MoS<sub>2</sub> suspension at different pH values was also measured using a Malvern Zetasizer. The pH of the MoS<sub>2</sub> suspension was adjusted using 0.1 M sodium hydroxide (NaOH) and hydrogen chloride (HCl) solutions. The surface functional groups of the MoS<sub>2</sub> nanosheets were characterized using a Thermo Scientific K-alpha XPS spectrometer (Thermo Fisher Scientific, Ashville, NC, USA). Scanning electron microscopy (SEM) images were obtained using a Hitachi SU8010 fieldscanning electron microscopy system (Hitachi High Technologies, Tokyo, Japan). The material crystallographic structure was analyzed using an X'Pert PRO Alpha-1 diffraction system (45 kV, 40 mA). Note that the X-ray diffraction (XRD) pattern of the base PVDF membrane substrate exhibits peaks that can potentially overlap with the peaks of MoS<sub>2</sub>. Therefore, the MoS<sub>2</sub> nanosheets were vacuum-filtered on a porous Anodisc alumina oxide membrane, which is 47 mm in diameter and 0.2 µm in pore size (Whatman Nucleopore Corp., Clifton, NJ, USA), for XRD analysis.

Evaluation of Molybdenum Disulfide Membrane Performance. The water permeability, water flux, and solute rejection of the synthesized MoS2 membranes were investigated using an Amicon model 8010 dead-end filtration cell (Millipore Corp., Billerica, MA, USA). The effective testing area of the filtration cell was 4.1 cm<sup>2</sup>. The membrane coupon was first loaded into the stirred filtration cell and compacted under a pressure of 2 bar for 60 min using deionized (DI) water. The applied hydraulic pressure was then reduced to 1 bar to determine the membrane water permeability. The measurement was run for 60 min, and the membrane water permeability was calculated

$$A = \frac{J_{\rm W}}{\Delta P} \tag{1}$$

where A is the membrane water permeability,  $J_{W}$  is the water flux, and  $\Delta P$  is the applied hydraulic pressure.

The membrane water flux and salt rejection were also characterized using the filtration cell. The membrane water flux was first measured using DI water as the feed solution. Before the measurement, the membrane was compacted under a hydraulic pressure of 2 bar for 60 min. Then, the pressure was decreased to a predetermined value, and the water flux measurement was run for 60 min. After that, the hydraulic pressure was increased gradually, and the water flux was measured for 60 min for each predetermined hydraulic pressure value. Finally, the hydraulic pressure was increased to 2 bar, and the corresponding water flux was measured.

The membrane rejection of NaCl and Na<sub>2</sub>SO<sub>4</sub> was investigated. For NaCl, feed solutions with a few different concentrations (1, 5, and 10 mM) were prepared, and the rejection of each solution was tested. For Na<sub>2</sub>SO<sub>4</sub>, a 1 mM feed solution was prepared and used for the experimental measurement. For each feed solution, the membrane was first compacted under a hydraulic pressure of 2 bar for 60 min. Then, the hydraulic pressure was reduced to a lower value to measure the salt rejection, and the measurement was run for 60 min. After that, the hydraulic pressure was increased to a predetermined value, and for each hydraulic pressure value, the salt rejection was measured. Finally, the hydraulic pressure was increased to 2 bar, and the salt rejection under such pressure was also measured. In addition, the membrane water flux was also measured under each hydraulic pressure. The salt rejection (R)was determined by

$$R = \left(1 - \frac{C_{\rm p}}{C_{\rm f}}\right) \times 100\% \tag{2}$$

where  $C_f$  is the concentration of salt in the feed solution and  $C_p$  is the concentration of salt in the permeate. The concentrations of the salt solutions were determined using a conductivity meter.

Besides, the membrane mean pore size  $(d_p)$  was also measured using the same filtration cell. Polyethylene glycol (PEG) solutions with different molecular weights  $(M_W s)$  (Table S1) were used to measure  $d_{s}$ , and a detailed description is shown in the Supporting Information (SI1). The membrane interlayer spacing obtained from XRD measurements is an important parameter for understanding water and ion transport inside the MoS2 nanosheets; however, previous studies suggested that defects inevitably exit inside the 2D nanosheet membranes. <sup>11,36</sup> These defects are formed due to the imperfect stacking during the fabrication of the membranes, and they can be larger than the membrane interlayer spacing. Using the membrane mean pore size obtained from the PEG rejection tests, these defects can be successfully taken into account and their influence on mass transport can be well studied.

Modeling of Salt Ion Transport Across the Membrane. A mathematical framework was constructed to describe the mass transport process (the concentration profile of the MoS2 membrane is shown in Figure S1). According to previous studies, the diffusion rate of charged species is affected when the EDL thickness is comparable to the size of the nanochannel.<sup>37</sup> Additionally, the concentration of the charged species is not homogeneous inside the EDL. A parameter named the exclusion-enrichment coefficient ( $\beta$ ) was defined to quantify the influence of the extension of the EDL on the concentration and diffusion rate of the charged species.<sup>30</sup> The coefficient can be expressed

$$\beta = \frac{C_{\text{eff}}}{C} = \frac{P_{\text{eff}}}{P} \tag{3}$$

where  $C_{\text{eff}}$  is the effective concentration, C is the bulk concentration,  $P_{\text{eff}}$ is the effective permeability (by diffusion), and P is the permeability when the EDL thickness is negligible (thus, the influence of the electrostatic interactions on solute diffusion is negligible). The extension of the EDL results in the exclusion of coions and the enrichment of counterions; the  $\beta$  of the counterions is larger than unity, and the  $\beta$  of the coions is smaller than unity. Regarding the salt transport across the membrane, since electroneutrality needs to be fulfilled, the transport rate of the coions equals that of the counterions. Thus, the transport rate of salt can be represented by that of the coions for a 1-1 salt. In this regard, the exclusion-enrichment coefficient of the coions is examined.

The salt is transported across the membrane by both diffusion and convection, 11 and diffusion is influenced by the exclusion-enrichment coefficient, as discussed. In addition, steric hindrance needs to be considered since the Stokes radius of the ions can be at the same order of magnitude as the dimension of the nanochannels inside the MoS<sub>2</sub>

membrane. The flux of the coion  $(J_{i,co})$  (as well as counterions) equals that of the salt  $(J_S)$  for a 1-1 salt and can be calculated using the following equation

$$J_{\rm S} = -\beta D_{\rm ip} \frac{\mathrm{d}c_{\rm co}}{\mathrm{d}z} + K_{\rm i} J_{\rm W} c_{\rm co} \tag{4}$$

where  $D_{\mathrm{ip}}$  is the effective coion diffusion coefficient in the membrane pores,  $c_{co}$  is the concentration of the coion,  $K_{ic}$  is the hindrance factor for convection, and  $J_{\rm W}$  is the water flux.  $D_{\rm ip}$  can be given by

$$D_{\rm ip} = K_{\rm id} D_{\rm i} \tag{5}$$

where  $K_{\rm id}$  is the hindrance factor for diffusion and  $D_{\rm i}$  is the ion diffusion coefficient in bulk solution. The estimation of the hindrance factors is shown in the Supporting Information (SI2). The boundary conditions can be established as follows

$$z = 0$$
,  $c_{co} = c_{co,0}$  (6a)

$$z = t, \ c_{\rm co} = c_{\rm co,t} \tag{6b}$$

where t is the membrane thickness,  $c_{\mathrm{co,0}}$  is the coion concentration inside the membrane at the membrane and feed solution interface, and  $c_{\mathrm{co,t}}$  is the coion concentration inside the membrane at the membrane and permeate interface. As shown in Figure S1, the ion concentrations inside the membrane are higher at the membrane and feed solution interface than at the membrane and permeate interface. A generalized equation for salt flux across the membrane can be obtained by combining eqs 4 and 5 and using eqs 6aa and 6b6b as the boundary

$$J_{\rm S} = \frac{K_{\rm i}J_{\rm W} \left[ c_{\rm co,0} \, \exp\left(\frac{K_{\rm i}J_{\rm W}t}{\beta D_{\rm ip}}\right) - c_{\rm co,t} \right]}{\exp\left(\frac{K_{\rm i}J_{\rm W}t}{\beta D_{\rm ip}}\right) - 1}$$

$$(7)$$

In addition, the concentration profiles of the coion and counterion inside the membrane can be calculated based on eq 4, and the detailed calculation of the concentration profiles is shown in the Supporting Information (SI4).

The electrical potential  $(\psi)$  inside the nanochannel can be calculated using the Poisson-Boltzmann differential equation<sup>3</sup>

$$\frac{\partial^2 \psi}{\partial x^2} = \frac{2Fc}{\varepsilon_0 \varepsilon_r} \sinh \left( \frac{F}{\psi RT} \right) \tag{8}$$

where x is the relative radial position inside the membrane nanochannel  $(0 \le x \le r_p)$ , F is the Faraday constant, R is the ideal gas constant, T is the absolute temperature,  $\varepsilon_0$  is the permittivity of vacuum, and  $\varepsilon_r$  is the dielectric constant of the medium. The electrical potential depending on the radial position (x) inside the nanochannel can be determined using the following boundary conditions

$$\psi_{x=0} = \psi_0 \tag{9a}$$

$$\psi_{x=2r_{p}} = \psi_{0} \tag{9b}$$

where  $\psi_0$  is the surface potential. The Debye–Huckel approximation can be used to obtain a simpler expression of the electrical potential across the membrane nanochannel

$$\frac{\psi_{x}}{\psi_{0}} = \frac{\cosh\left(\frac{r_{p} - x}{\lambda_{D}}\right)}{\cosh\left(\frac{r_{p}}{\lambda_{D}}\right)} \tag{10}$$

The relative electrical potential (compared to the surface potential of the nanochannel wall,  $\psi_0$ ) can be obtained using eq 10. The EDL thickness, which can be characterized by the Debye length  $(\lambda_D)$ , is related to the ion concentrations

$$\lambda_{\rm D} = \left(\frac{e_{\rm r}\epsilon_0 k_{\rm B}T}{2N_{\rm A}\epsilon^2 I}\right)^{1/2} \tag{11}$$

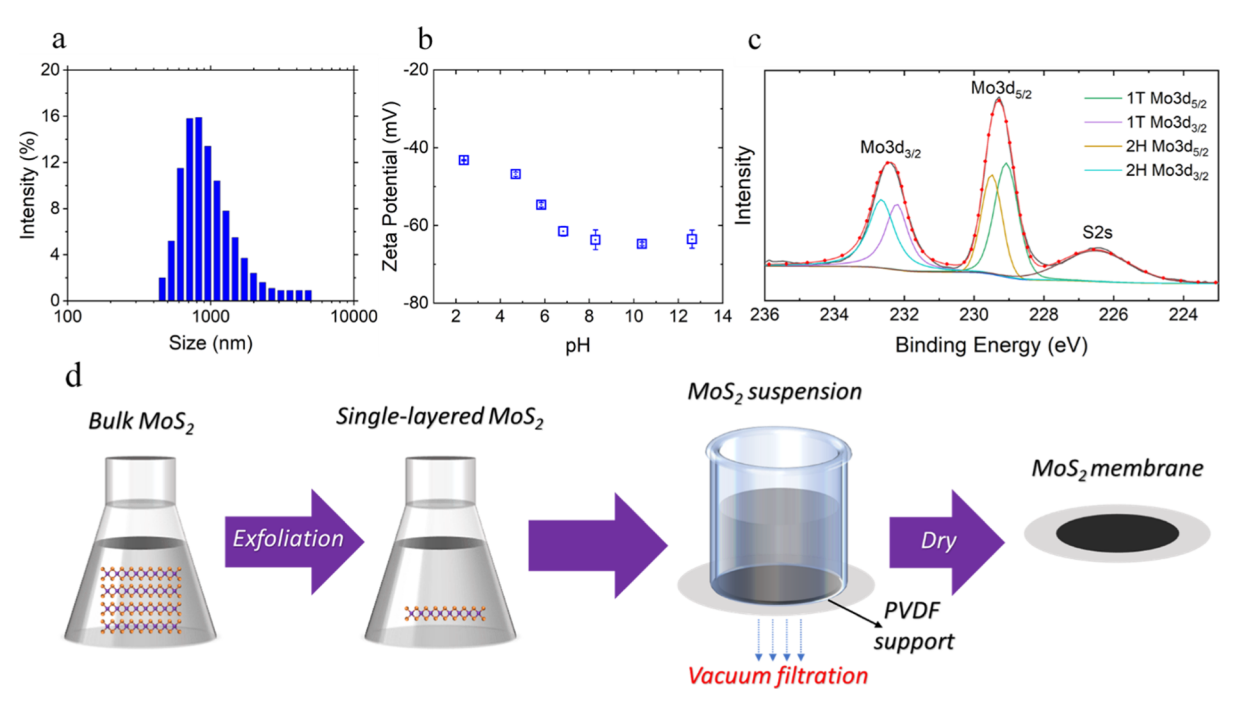


**Figure 1.** (a) Hydrodynamic size distribution of the as-prepared  $MoS_2$  nanosheets. (b) Zeta potential of the  $MoS_2$  nanosheet suspension at different pH values. (c) XPS spectra of exfoliated  $MoS_2$  nanosheets, indicating the presence of both the 1T phase and 2H phase of  $MoS_2$ . (d) Schematic illustration showing the fabrication procedure of the  $MoS_2$  membrane.

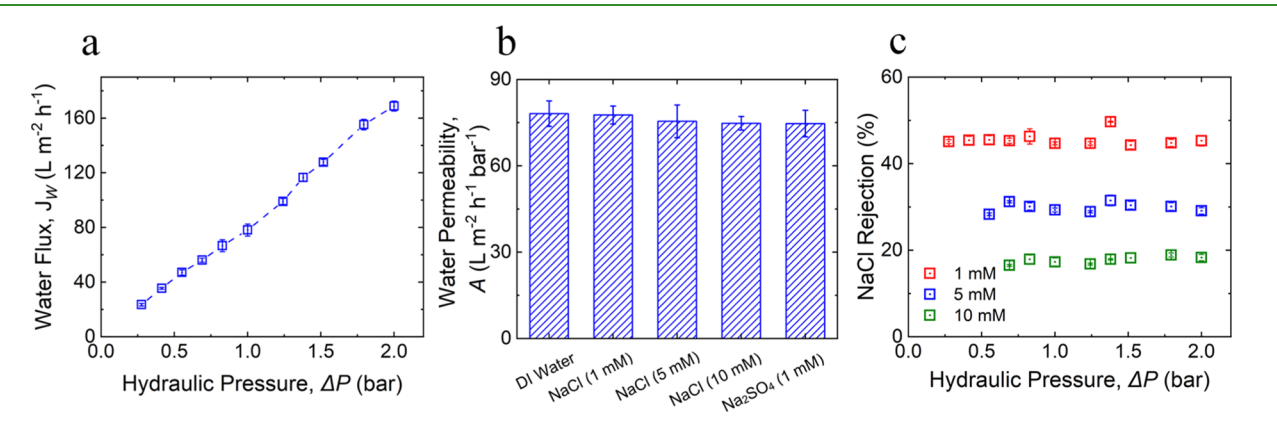


Figure 2. (a) MoS<sub>2</sub> membrane pure water flux as a function of the applied hydraulic pressure. (b) MoS<sub>2</sub> membrane water permeability measured using different feed solutions. The solution osmotic pressure was considered when calculating the membrane water permeability. (c) Membrane NaCl rejection under different hydraulic pressure values. Three NaCl solutions with different concentrations (1, 5, and 10 mM) were used as the feed solution

where  $k_{\rm B}$  is the Boltzmann constant,  $N_{\rm A}$  is Avogadro's number, e is the electron charge, and I is the ionic strength. In addition, the surface potential can be estimated using the measured zeta potential ( $\xi$ ) by assuming that the zeta potential was measured at a distance s (s=1 nm) $^{17,41}$ 

$$\psi_0 = \frac{\xi}{\exp\left(-\frac{s}{\lambda_D}\right)} \tag{12}$$

Note that the measured zeta potential represents the potential at the shear plane rather than the potential on the surface itself.

# RESULTS AND DISCUSSION

Material and Membrane Characterization. The average hydrodynamic size of the exfoliated MoS<sub>2</sub> nanosheets was determined to be 825 nm by dynamic light scattering, as shown in Figure 1a. The zeta potential of the MoS<sub>2</sub> suspension was measured at different pH values (2 to 13), a negative zeta

potential was observed throughout the entire measured pH range, and generally, the zeta potential decreased with increasing pH (Figure 1b). The XPS analyses (Figure 1c) indicate that exfoliated  $MoS_2$  contains a mixture of the metallic 1T phase and semiconducting 2H phase.<sup>12</sup>

The  $MoS_2$  membranes were fabricated using a vacuum filtration method (Figure 1d), and the synthesized membrane had a layered structure (as illustrated by the cross-sectional SEM image shown in Figure S3). The successful deposition of the  $MoS_2$  nanosheets onto the surface of the porous PVDF membrane can be confirmed by comparing the morphologies before and after vacuum filtration (Figures S2 and S3).  $MoS_2$  membranes with different thicknesses were synthesized by varying the volume of the  $MoS_2$  suspension. As listed in Table S2, the thickness of the membrane increases with increasing  $MoS_2$  suspension loading. The thickness of  $MoS_2$ -6 was determined to be 3.6  $\mu$ m from the cross-sectional SEM image

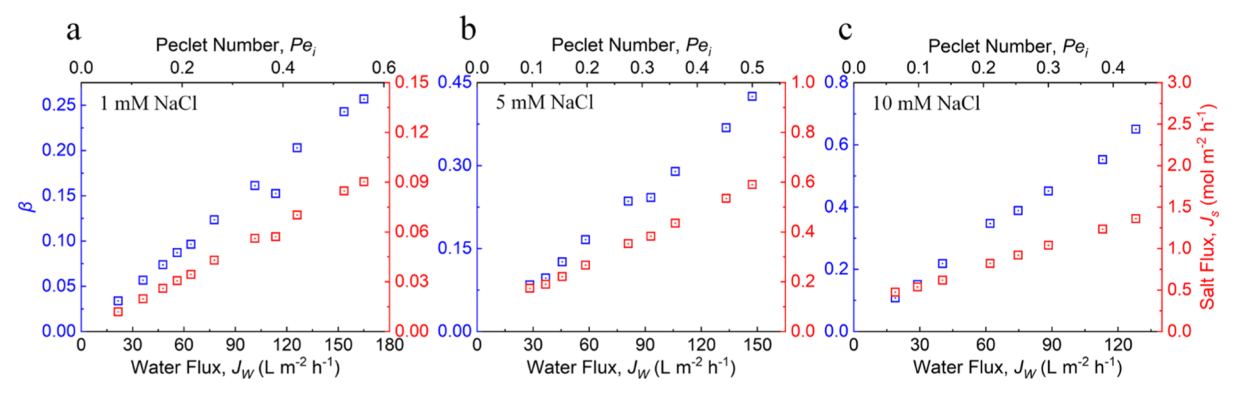


**Figure 3.** Change in the exclusion-enrichment coefficient ( $\beta$ ) of coions (Cl<sup>-</sup>) and membrane salt flux ( $I_S$ ) with increasing membrane water flux ( $I_W$ ) (bottom horizontal axis) and Péclet number ( $Pe_i$ ) of coions ( $Cl^-$ ) (top horizontal axis) with NaCl feed solution concentrations of (a) 1, (b) 5, and (c) 10 mM.

(Figure S3). By assuming that the measured thickness of the membrane increases proportionally with increasing MoS<sub>2</sub> suspension loading, the thickness of the other membranes can be determined (Table S2). The XRD pattern of the as-prepared MoS<sub>2</sub> membrane (Figure S4a) shows a relatively strong (001) peak, from which the corresponding interlayer spacing was determined to be 1.1 nm. This signifies the metallic 1T phase of the membrane; in contrast, the thermodynamically stable 2H phase results in a strong peak in bulk MoS<sub>2</sub> (Figure S4b), suggesting an interlayer spacing of 0.62 nm. 42

Membrane Water and Salt Transport Properties. The water permeability of the MoS<sub>2</sub> membranes was measured using DI water as the feed solution. The membrane water permeability decreased with increasing membrane thickness (Figure S5). MoS<sub>2</sub>-1 and MoS<sub>2</sub>-6 possessed a water permeability of 687.8 L m<sup>-2</sup> h<sup>-1</sup> bar<sup>-1</sup> (LMH-bar) and 78.1 LMH-bar, respectively. To reduce the possibility of pinholes and defects, MoS2 membranes with relatively large thicknesses are desired to analyze the transport properties. 43 In this regard, MoS<sub>2</sub>-6 with a measured thickness of 3.6 µm (Table S2) was chosen for further investigation. For simplification, the MoS2 membrane was then used to represent the MoS2-6 membrane during the discussion, unless stated otherwise. The water flux using DI water as the feed solution was also measured under different hydraulic pressures (up to 2 bar). From Figure 2a, the membrane water flux increased linearly with increasing hydraulic pressure, which indicates that the MoS<sub>2</sub> membrane is physically stable, and the nanochannels inside the membrane are rigid enough to withstand the applied pressure in this study. In addition, the membrane water permeability was also estimated using different feed solutions under a hydraulic pressure of 1 bar. The water permeability was calculated by considering the solution osmotic pressure  $(\Delta \pi)$ 

$$A = \frac{J_{\rm W}}{\Delta P - \Delta \pi} \tag{13}$$

As shown in Figure 2b, the membrane water permeability was constant regardless of the feed solution composition. This suggests that the nanochannels inside the MoS2 membrane are stable in the solutions and are not influenced by the change in the solution composition or ionic strength.<sup>21</sup>

The measured NaCl salt rejection values of the MoS<sub>2</sub> membrane under various hydraulic pressures are shown in Figure 2c. For each feed NaCl solution concentration, the membrane rejection was independent of the change in hydraulic pressure (up to 2 bar), with only a slight fluctuation observed. It

is also obvious from the figure that with the increase in the feed NaCl solution concentration, the membrane rejection decreased abruptly. When the feed NaCl solution concentration was 1 mM, the membrane rejection was approximately 45%. However, when the concentration was increased to 10 mM, the membrane rejection rapidly decreased to approximately 17%. The membrane mean pore size was determined by measuring the rejection of PEG under a hydraulic pressure of 2 bar. The rejection results are shown in Figure S6. Based on the results, the mean pore size of the MoS<sub>2</sub> membrane was determined to be 6.37 nm.

**Enhancement Enrichment Effect under Different Conditions.** To better understand the salt rejection performance of the MoS<sub>2</sub> membrane, the exclusion-enrichment coefficient  $(\beta)$  of the coion  $(Cl^{-})$  was calculated using eq 7. In addition, the Péclet number of the coion  $(Pe_i)$  was also estimated for the different experimental conditions (different hydraulic pressures and feed solution concentrations). The Péclet number is defined as the ratio of the effective convection to the effective diffusion of an ion in membrane nanochannels<sup>44</sup>

$$Pe_i = \frac{J_{\rm W}K_{\rm ic}L_{\rm e}}{D_{\rm ip}} \tag{14}$$

where  $L_{\rm e}$  is the effective thickness of the MoS<sub>2</sub> membrane. The effective thickness is defined as the ratio of the membrane thickness to the membrane porosity, 45 which can be estimated based on the Hagen-Poiseuille equation 46

$$J_{\rm W} = \frac{r_{\rm p}^2 \Delta P}{8\mu L_{\rm e}} \tag{15}$$

where  $r_{\rm p}$  is the effective membrane pore radius and  $\mu$  is the solution viscosity. The membrane pure water flux under different hydraulic pressure values was used to calculate the effective membrane thickness, and the average value was taken (Table S3).

Since the Péclet number reveals the relative importance of convection and diffusion, by calculating the Péclet number, the effect of convective mass transport on the enhancement enrichment effect can also be examined. Figure 3 shows the change in the exclusion-enrichment coefficient ( $\beta$ ) of coion and membrane salt flux  $(J_S)$  with increasing membrane water flux for different NaCl feed solution concentrations. It is obvious that for all the feed solution concentrations, with the increase in the water flux, the salt (NaCl) flux also increases. In addition, the increase in the water flux means that the contribution of

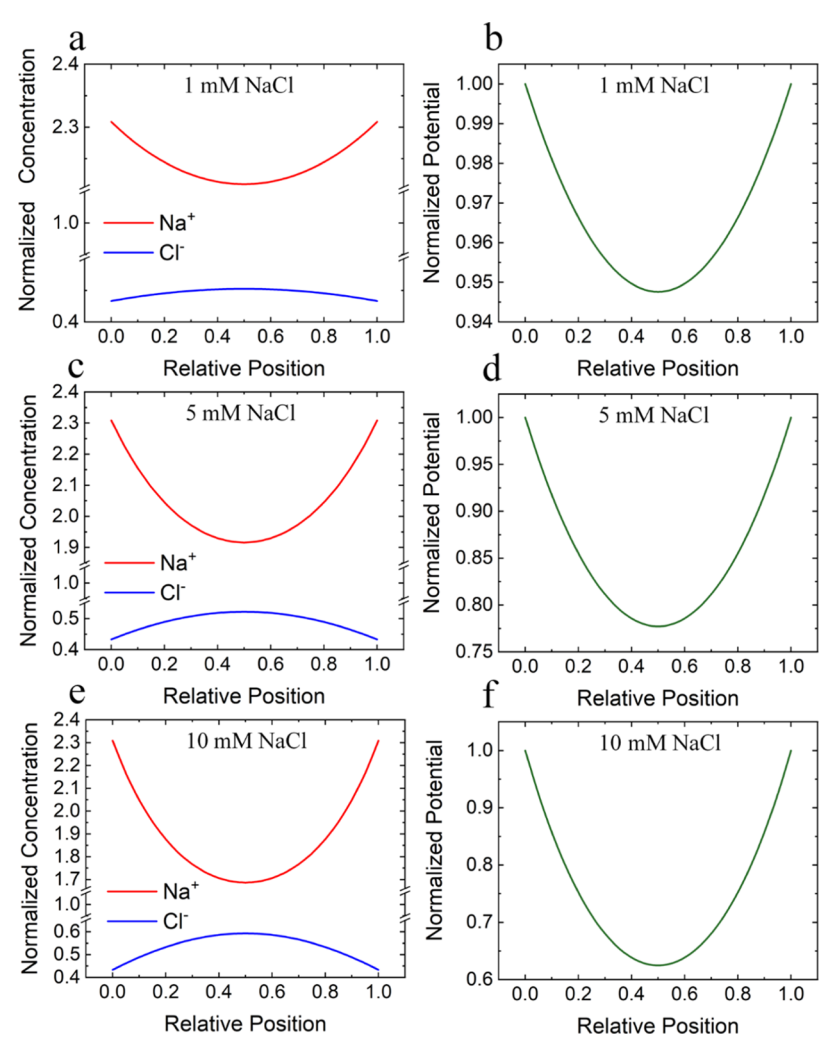


Figure 4. Radial concentration profiles across the  $MoS_2$  membrane nanochannel with NaCl feed solution concentrations of (a) 1, (c) 5, and (e) 10 mM. The concentration is normalized relative to the bulk ion concentrations inside the nanochannel. Radial electrical potential across the  $MoS_2$  membrane nanochannel with NaCl feed solution concentrations of (b) 1, (d) 5, and (f) 10 mM. The electrical potential is normalized relative to the surface potential (the electrical potential at positions 0 and 1). An average membrane nanochannel diameter of 6.37 nm was used.

convection to the overall salt transport increases, which can be indicated by the increase in  $Pe_i$ . The increase in  $\beta$  with the increase in the membrane water flux (or the increase in  $Pe_i$ ) implies that the exclusion-enrichment coefficient of the coion became weaker. From eq 4, the exclusion-enrichment effect reduces the coion diffusion rate by introducing a retardation factor ( $\beta \leq 1$ ). However, it was previously uncertain how convection influences the exclusion-enrichment effect. In Figure 3a,  $\beta$  increased from 0.03 to 0.26 when the water flux increased from 21.6 to 165.0 LMH ( $Pe_i$  increased from 0.07 to 0.56), suggesting that the coions diffuse faster when the water flux was larger. The increased salt flux with increasing Péclet number was a result of both enhanced diffusive (by increasing  $\beta$ ) and convective (by increasing water flux) mass transport.

The feed solution concentration has a substantial influence on the exclusion-enrichment effect. For example, a water flux of 100 LMH resulted in a Péclet number of approximately 0.34 for the NaCl solution; under such conditions, when the NaCl feed solution concentration was 1, 5, and 10 mM, the exclusion-enrichment coefficient ( $\beta$ ) was estimated to be approximately 0.16, 0.25, and 0.50, respectively (Figure 3). The increased  $\beta$  value obtained with increasing feed solution concentration indicates that the exclusion-enrichment effect becomes weaker

at higher feed solution concentrations. It was demonstrated that the overlapping EDL can increase the diffusion time of charged species across the nanochannels; additionally, a further increase in the EDL thickness (by decreasing the solution concentration and ionic strength) further reduced the diffusive solute flux by enhancing the electrostatic interactions between the charged species and the walls of the nanochannels.<sup>30</sup> In this study, at lower feed solution concentrations, the ion concentrations inside the membrane were also lower, and the EDL thickness was larger, which led to enhanced electrostatic interactions and lowered diffusive ionic flux.

Note that the exclusion-enrichment effect is also ion-specific. The exclusion-enrichment coefficients were also calculated when the 1 mM  $\rm Na_2SO_4$  solution was used as the feed solution. From Figure S7, the Péclet number was estimated to be 0.65 when the water flux was set to 100 LMH, which was different from the case when the feed was the NaCl solution. The abovementioned difference was caused by the different steric hindrances resulting from the different coions (since the different ions have different radii, as shown in Table S4), according to eq 14. In addition, it should be noted that the  $\rm Na_2SO_4$  solution was used for experimental insights only, as the

mass transport models developed in this study are limited to 1-1 salt solutions.

Mechanistic Insights. The exclusion-enrichment effect is largely influenced by the ion concentrations inside the MoS<sub>2</sub> membrane, as discussed. Hence, the ion concentration profiles were estimated to further study the mechanisms responsible for ion transport through the MoS2 membrane. Steric exclusion and Donnan exclusion were considered during the estimation of the ion concentrations across the membrane, and a detailed description of the calculation procedure is listed in the Supporting Information (SI4). According to the ion concentration profiles across the MoS<sub>2</sub> membrane (Figure S8), the counterion (Na<sup>+</sup>) concentration is higher than the coion (Cl<sup>-</sup>) concentration since the MoS2 membrane has a negative volumetric charge density. Additionally, a concentration gradient is formed across the membrane for both the counterion and coion.

The change in electrical potential across the membrane nanochannel can be estimated using eq 10. Furthermore, the local ion concentration change across the nanochannel ( $0 \le x \le$  $r_{\rm p}$ ) can also be estimated using the local electrical potential.<sup>47</sup> The calculated concentration profiles (Figure S8) can identify the local ion concentrations across the MoS<sub>2</sub> membrane thickness (the z-direction); however, the concentration change across the membrane nanochannel (along the x-direction) cannot be seen from the concentration profiles, and thus, the exclusion-enrichment effect cannot be fully explained. Here, the ion concentration change across the membrane nanochannel was calculated using the Boltzmann distribution<sup>38</sup>

$$\frac{c_x}{c} = \exp\left(-z_i e \frac{\psi_x}{k_{\rm B}T}\right) \tag{16}$$

where  $z_i$  is the valence of the ion.

The (normalized) concentration and potential distributions along the membrane nanochannel are shown in Figure 4 for the different feed solution concentrations. From the figure, the electrostatic exclusion of coions and enrichment of the counterions due to the extension of the EDL are indicated by the change in the radial concentrations of the ions. The counterion concentration is enhanced near the surface of the nanochannel and gradually decreases when moving close to the center of the nanochannel. However, the counterion concentration is still higher than the bulk concentration. For the coions, their concentration is the lowest on the surface of the nanochannel and gradually increases when moving close to the center of the nanochannel. Whereas the coion concentration at the center of the nanochannel is still lower than the bulk concentration. The weakening of the exclusion-enrichment effect with the increase in the feed solution concentration can also be observed from the change in the ion concentrations. When the NaCl feed solution concentration is 1 mM (Figure 4a), the counterion and coion concentrations at the center of the nanochannel are 2.21 and 0.45 times the bulk concentrations, respectively. As the feed NaCl solution concentration increases to 10 mM (Figure 4e), the counterion and coion concentrations at the center of the nanochannel become 1.69 and 0.59 times the bulk concentrations, respectively. More importantly, when the feed NaCl solution concentration is 500 mM (Figure S9), the ion concentrations in most parts of the nanochannel equal the bulk concentration, implying the absence of the exclusionenrichment effect in these positions.

The weakening of the exclusion-enrichment effect with increasing NaCl feed solution concentration can also be indicated by the degree of electrical potential decay. When the NaCl feed solution concentration equals 1, 5, and 10 mM, the electrical potential at the center of the nanochannel becomes 0.95, 0.78, and 0.62 times the surface electrical potential, respectively (Figure 4b,d,f). However, when the feed solution concentration increases to 500 mM (Figure S9), the electrical potential at the center of the nanochannel becomes almost zero, suggesting a much faster potential decay rate under such conditions, that is, at the central part of the nanochannel, the coions can transport freely with no electrostatic interactions that need to be considered.

Note that many previous studies assumed that the interlayer spacing of 2D nanosheet membranes acts as free space for mass transport, and the membrane molecular cutoff can be controlled by adjusting the membrane interlayer spacing. 16,25 However, based on the results obtained from this study, there is a difference between the measured MoS2 membrane mean pore size (using PEG rejection tests) and the determined interlayer spacing (using XRD results). This suggests that defects inevitably form during poorly controlled membrane fabrication processes, and these defects can have a non-negligible influence on water and solute transport across the membrane. 36,48 From Figure 4, it is clear that the nanoporous defects (size of a few nanometers) caused by the nonperfect stacking of the 2D nanosheet during the membrane fabrication can maintain a quite strong exclusion-enrichment effect. The ion transport inside the interlayer spacing can have an even stronger exclusionenrichment effect since the interlayer spacing is even smaller than the membrane mean pore size. To further evaluate how the larger defects (with diameters larger than 10 nm) influence the exclusion-enrichment effect inside the 2D MoS<sub>2</sub> membrane, we calculated the normalized concentration distributions along the membrane nanopores of different sizes. As shown in Figure S10, nanopores with a diameter of 10 or 20 nm can effectively enrich counterions and exclude coions. The exclusion-enrichment effect only starts to diminish when the diameter of the nanopore increases to larger than 50 nm. Thus, a strong exclusionenrichment effect can still be maintained inside defects with sizes of a few tens of nanometers in 2D nanosheet membranes.

An alternative way to describe the mass transport across the MoS<sub>2</sub> membrane is using the extended Nernst-Planck equation, which accounts for diffusion, convection, and electromigration<sup>4</sup>

$$J_{i} = -D_{ip} \frac{\mathrm{d}c_{ci}}{\mathrm{d}z} + K_{ic} J_{W} c_{i} - z_{i} c_{i} K_{ic} \frac{F}{RT} \frac{\mathrm{d}\psi}{\mathrm{d}z}$$

$$\tag{17}$$

where  $J_i$  is the ion flux (which equals the salt flux  $J_S$  in this study). The detailed description of the Donnan steric pore model (DSPM) based on the extended Nernst-Planck equation is listed in the Supporting Information (SI5). The salt (NaCl) flux across the membrane was estimated using the DSPM and compared with the experimental values (Figure S11). From the figure, when the water flux (and Péclet number) is low, there is a huge difference between the model and experimental salt flux values; with the increase in the water flux, the difference becomes smaller. Generally, the DSPM overestimated the salt flux across the membrane. This might be caused by the fact that the DSPM, which is based on the extended Nernst-Planck equation, cannot comprehensively capture the physics of the solute transport process through the membrane. In the case of the 2D membranes, the extension of the EDL largely influences the interactions between the solute and the wall of the

nanochannel; however, the DSPM is incapable of fully accounting for the influence of the EDL on the ion transport. When the water flux is low, the exclusion-enrichment effect is strong, and there is a huge difference between the model and experimental salt flux values (the difference can be larger than 60%). With the increase in the water flux, the exclusionenrichment effect becomes weaker due to the enhancement of convection. First, the increase in water flux can significantly increase the overall ion flux by enhancing convective transport of ions. Second, the increased water flux may displace the shear plane. As a result, the difference between the model and experimental salt flux values becomes smaller.

The exclusion-enrichment coefficient  $(\beta)$  can also be calculated theoretically by estimating the average radial coion concentration over the MoS<sub>2</sub> membrane nanochannel<sup>30</sup>

$$\beta = \frac{1}{r_{\rm p}} \int_0^{r_{\rm p}} \exp \left( -z_{\rm i} e^{\frac{\xi \cosh\left(\frac{r_{\rm p}}{2} - x\right)}{\lambda_{\rm D}}} \frac{1}{k_{\rm B}T} \right) dx$$
(18)

Note that the exclusion-enrichment coefficient calculated using the abovementioned equation does not consider the influence of convective mass transport. Hence, the estimated coefficients are the theoretically lowest values, and the experimental values obtained from the pressure-driven membrane system measurements should be higher than the calculated values. As shown in Figure 5, the theoretical

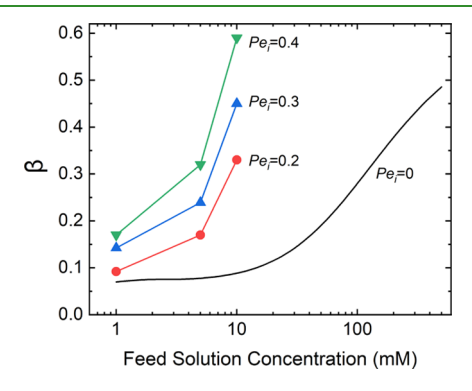


**Figure 5.** Change in the exclusion-enrichment coefficient ( $\beta$ ) of coions (Cl<sup>-</sup>) with increasing NaCl feed solution concentration for different Péclet numbers  $(Pe_i)$  of coions  $(Cl^-)$ . The exclusion-enrichment coefficient ( $\beta$ ) when the Péclet number ( $Pe_i$ ) equals 0 (the black curve) was calculated using eq 15. The exclusion-enrichment coefficient  $(\beta)$ values when the Péclet number (Pei) is larger than 0 (the dots connected by straight lines) were obtained using eq 7 with experimental salt and water flux values.

exclusion-enrichment coefficient  $(\beta)$  with a Péclet number (Pei) of 0 increases with increasing NaCl feed solution concentration. The exclusion-enrichment coefficient values fitted using the experimental data also increase with increasing feed solution concentration; at the same feed solution concentration, a larger Pei value leads to a larger exclusionenrichment coefficient. It is thus concluded that the theoretical values are in accordance with the experimental fitted values in this study. Additionally, both the shrinkage of the EDL thickness (i.e., increase in the feed solution concentration) and increase in convective mass transport can weaken the exclusion-enrichment effect.

Implications on 2D Membrane Design and Applications. 2D nanosheet membranes have been extensively studied for water and wastewater treatment in recent years; however, the transport mechanisms inside 2D nanosheet membranes are far from being fully understood. This study shows that due to the well-defined structure and the spatial confinement inside the nanochannels of the 2D nanosheet membrane, the EDL inside the membrane occupies a significant portion of space and can overlap in many cases. The results from this study indicate that the extension of the EDL inside the nanochannels of MoS<sub>2</sub> can significantly influence ion transport by inducing a strong exclusion-enrichment effect. Although nanofluidic devices that can completely block ions by steric exclusion are possible, 50 the stacking of the 2D nanosheet membranes will inevitably form numerous nanochannels that are large enough for ion and molecular transport. The electrostatic interaction between the ions (and charged molecules) and the nanochannels can be utilized to design membrane processes with enhanced solute retention. For example, low pressure-driven processes can be used to achieve high retention of charged species, while energyefficient solute-solute separation can potentially be achieved

using 2D nanosheet membranes.<sup>51</sup>

Nevertheless, it is also beneficial to recognize the limitations of 2D nanosheet membranes. It is a daunting task to use 2D nanosheet membranes for seawater desalination and achieve the performance and efficiency of state-of-the-art TFC membranes.<sup>52</sup> Under such high ionic strength, steric exclusion is like to be the sole ion retention mechanism since the EDL thickness is negligible compared to the size of the nanochannel, and the coions can freely transport across the nanochannels with little electrostatic repulsion. In addition, the existence of defects increases the water flux and thus further weakens the exclusionenrichment effect by increasing the convective mass transport. Hence, it is important to screen the appropriate applications suited to the properties of 2D nanosheet membranes. The retention of charged large molecules under relatively low applied hydraulic pressures can be a promising application for these membranes. The large size of the large molecule can increase the steric exclusion of the membranes, which is an additional benefit. In addition, the unique properties of 2D nanosheet membranes might be translated to applications such as contaminant adsorption<sup>53</sup> and degradation.<sup>54</sup> The fast water transport rate and the confinement effect can potentially lead to high-efficiency contaminant adsorption and degradation. Additionally, the strong exclusion-enrichment effect induced by the restacking of 2D nanosheets can increase the electrostatic interaction between the nanochannel and target species.

Since the exclusion-enrichment effect is highly related to the surface properties of the membrane nanochannel, synthesizing membranes using 2D nanosheets with increased surface charge densities can enhance the exclusion-enrichment effect. This can be carried out by introducing additional functional groups onto the surface of the 2D materials. 19 Alternatively, using charged molecules as spacers between 2D nanosheets is an effective approach to increase the volumetric charge density of the overall membrane. 55 Regarding the membrane fabrication process, bottom-up approaches with molecular-level precision can significantly increase the membrane transport properties by reducing the possibility of defects. Although the exclusionenrichment effect can still be maintained inside defects with diameters of tens of nanometers, a 2D nanosheet membrane with well-regulated nanochannels can boost both steric exclusion and electrostatic exclusion to ensure an even higher performance of the membrane.

# CONCLUSIONS

This study initiates a quantitative investigation of the exclusionenrichment effect in a 2D MoS<sub>2</sub> membrane and its influence on salt transport. In addition, how convective mass transport can affect the exclusion-enrichment effect in the membrane is quantified. The conclusions obtained from this study have profound meaning toward the future design and application of 2D membranes in water and wastewater treatment. From this study, when treating feed solutions with relatively low total dissolved solids, the strong exclusion-enrichment effect of the MoS<sub>2</sub> membrane (indicated by the low  $\beta$  value) can significantly retard the diffusion of salt ions, especially when the applied hydraulic pressure is low. A direct consequence is that the retention of these charged species can be enhanced under such operating conditions. Based on the results from this study, charged solute separation under low pressure operations might be promising applications for the 2D nanosheet membranes.

# **ASSOCIATED CONTENT**

# Supporting Information

The Supporting Information is available free of charge at https://pubs.acs.org/doi/10.1021/acsami.1c03832.

Determination of the membrane mean pore size, calculation of hindrance factors, determination of membrane volumetric charge density, calculation of the concentration profile across the MoS<sub>2</sub> membrane, description of the Donnan steric pore model, concentration profile across the MoS2 membrane, surface and cross-sectional SEM images of the PVDF substrate membrane, cross-sectional SEM image of the MoS<sub>2</sub> membrane, XRD patterns of the as-prepared MoS<sub>2</sub> membrane and bulk MoS<sub>2</sub>, water permeability versus membrane thickness, PEG rejection of the MoS<sub>2</sub> membrane, change in the exclusion-enrichment coefficient ( $\beta$ ) of coions (SO<sub>4</sub><sup>2-</sup>) and membrane salt flux ( $J_S$ ) with increasing membrane water flux (J<sub>W</sub>) and Péclet number  $(Pe_i)$  of coions  $(SO_4^{2-})$ , concentration profiles of counterions (Na<sup>+</sup>) and coions (Cl<sup>-</sup>) in the MoS<sub>2</sub> membrane with different NaCl feed solution concentrations, radial concentration and electrical potential profiles across the MoS<sub>2</sub> membrane nanochannel with different NaCl feed solution concentrations, radial concentration profiles across the MoS<sub>2</sub> membrane pore with different nanopore diameters, model and experimental salt flux, Stokes diameter of PEG, synthesized MoS<sub>2</sub> membranes with different MoS<sub>2</sub> loadings and membrane thicknesses, basic properties of the MoS<sub>2</sub> membrane, radius of ions involved in this study, and surface charge density of MoS<sub>2</sub> and volumetric charge density of the MoS<sub>2</sub> membrane (PDF)

# AUTHOR INFORMATION

### **Corresponding Author**

Su Liu - School of Civil and Environmental Engineering, Georgia Institute of Technology, Atlanta, Georgia 30332, United States; Brook Byers Institute for Sustainable Systems, Georgia Institute of Technology, Atlanta, Georgia 30308, *United States;* © orcid.org/0000-0001-6459-5638; Email: suliu@gatech.edu

#### **Authors**

Xin Tong – School of Civil and Environmental Engineering, Georgia Institute of Technology, Atlanta, Georgia 30332, United States; Brook Byers Institute for Sustainable Systems, Georgia Institute of Technology, Atlanta, Georgia 30308, *United States*; orcid.org/0000-0002-2849-7683

Yangying Zhao - School of Civil and Environmental Engineering, Georgia Institute of Technology, Atlanta, Georgia 30332, United States; o orcid.org/0000-0002-2486-4845

Yongsheng Chen – School of Civil and Environmental Engineering, Georgia Institute of Technology, Atlanta, Georgia 30332, United States; o orcid.org/0000-0002-9519-2302

John Crittenden - School of Civil and Environmental Engineering, Georgia Institute of Technology, Atlanta, Georgia 30332, United States; Brook Byers Institute for Sustainable Systems, Georgia Institute of Technology, Atlanta, Georgia 30308, United States; o orcid.org/0000-0002-9048-7208

Complete contact information is available at: https://pubs.acs.org/10.1021/acsami.1c03832

The authors declare no competing financial interest.

#### ACKNOWLEDGMENTS

This study was supported by the Brook Byers Institute for Sustainable Systems, the Hightower Chair, and the Georgia Research Alliance at the Georgia Institute of Technology. This study was partially supported by the U.S. Department of Agriculture (award no. 2018-68011-28371), the National Science Foundation (award no. 1833988), and the National Science Foundation (award no. 1936928). This work was also performed in part at the Georgia Tech Institute for Electronics and Nanotechnology, which is supported by the National Science Foundation (grant ECCS-1542174). The views and ideas expressed herein are solely those of the authors and do not represent the ideas of the funding agencies in any form.

# REFERENCES

- (1) Vörösmarty, C. J.; McIntyre, P. B.; Gessner, M. O.; Dudgeon, D.; Prusevich, A.; Green, P.; Glidden, S.; Bunn, S. E.; Sullivan, C. A.; Liermann, C. R.; Davies, P. M. Global Threats to Human Water Security and River Biodiversity. Nature 2010, 467, 555-561.
- (2) Shannon, M. A.; Bohn, P. W.; Elimelech, M.; Georgiadis, J. G.; Mariñas, B. J.; Mayes, A. M. Science and Technology for Water Purification in the Coming Decades. *Nature* **2008**, 452, 301–310.
- (3) Wintgens, T.; Melin, T.; Schäfer, A.; Khan, S.; Muston, M.; Bixio, D.; Thoeye, C. The Role of Membrane Processes in Municipal Wastewater Reclamation and Reuse. Desalination 2005, 178, 1-11.
- (4) Amy, G.; Ghaffour, N.; Li, Z.; Francis, L.; Linares, R. V.; Missimer, T.; Lattemann, S. Membrane-Based Seawater Desalination: Present and Future Prospects. Desalination 2017, 401, 16-21.
- (5) Werber, J. R.; Osuji, C. O.; Elimelech, M. Materials for Next-Generation Desalination and Water Purification Membranes. Nat. Rev. Mater. 2016, 1, 16018.
- (6) Petersen, R. J. Composite Reverse Osmosis and Nanofiltration Membranes. J. Membr. Sci. 1993, 83, 81-150.
- (7) Elimelech, M.; Phillip, W. A. The Future of Seawater Desalination: Energy, Technology, and the Environment. Science 2011, 333, 712-
- (8) Gin, D. L.; Noble, R. D. Designing the Next Generation of Chemical Separation Membranes. Science 2011, 332, 674-676.
- (9) Geise, G. M.; Park, H. B.; Sagle, A. C.; Freeman, B. D.; McGrath, J. E. Water Permeability and Water/Salt Selectivity Tradeoff in Polymers for Desalination. J. Membr. Sci. 2011, 369, 130-138.

- (10) Wang, S.; Yang, L.; He, G.; Shi, B.; Li, Y.; Wu, H.; Zhang, R.; Nunes, S.; Jiang, Z. Two-Dimensional Nanochannel Membranes for Molecular and Ionic Separations. *Chem. Soc. Rev.* **2020**, *49*, 1071–1089.
- (11) Liu, S.; Tong, X.; Huang, L.; Hao, R.; Gao, H.; Chen, Y.; Crittenden, J. Study on the Transport Mechanism of a Freestanding Graphene Oxide Membrane for Forward Osmosis. *Environ. Sci. Technol.* **2020**, *54*, 5802–5812.
- (12) Hoenig, E.; Strong, S. E.; Wang, M.; Radhakrishnan, J. M.; Zaluzec, N. J.; Skinner, J.; Liu, C. Controlling the Structure of MoS2 Membranes via Covalent Functionalization with Molecular Spacers. *Nano Lett.* **2020**, *20*, 7844.
- (13) Hu, M.; Mi, B. Enabling Graphene Oxide Nanosheets as Water Separation Membranes. *Environ. Sci. Technol.* **2013**, 47, 3715–3723.
- (14) Hu, M.; Mi, B. Layer-by-Layer Assembly of Graphene Oxide Membranes via Electrostatic Interaction. *J. Membr. Sci.* **2014**, *469*, 80–87.
- (15) Mi, B. Graphene Oxide Membranes for Ionic and Molecular Sieving. *Science* **2014**, 343, 740–742.
- (16) Chen, L.; Shi, G.; Shen, J.; Peng, B.; Zhang, B.; Wang, Y.; Bian, F.; Wang, J.; Li, D.; Qian, Z.; Xu, G.; Liu, G.; Zeng, J.; Zhang, L.; Yang, Y.; Zhou, G.; Wu, M.; Jin, W.; Li, J.; Fang, H. Ion Sieving in Graphene Oxide Membranes via Cationic Control of Interlayer Spacing. *Nature* 2017, 550, 380–383.
- (17) Zheng, S.; Tu, Q.; Urban, J. J.; Li, S.; Mi, B. Swelling of Graphene Oxide Membranes in Aqueous Solution: Characterization of Interlayer Spacing and Insight into Water Transport Mechanisms. *ACS Nano* **2017**, *11*, 6440–6450.
- (18) Pendse, A.; Cetindag, S.; Lin, M. H.; Rackovic, A.; Debbarma, R.; Almassi, S.; Chaplin, B. P.; Berry, V.; Shan, J. W.; Kim, S. Charged Layered Boron Nitride-Nanoflake Membranes for Efficient Ion Separation and Water Purification. *Small* **2019**, *15*, 1904590.
- (19) Ries, L.; Petit, E.; Michel, T.; Diogo, C. C.; Gervais, C.; Salameh, C.; Bechelany, M.; Balme, S.; Miele, P.; Onofrio, N.; Voiry, D. Enhanced Sieving from Exfoliated MoS<sub>2</sub> Membranes via Covalent Functionalization. *Nat. Mater.* **2019**, *18*, 1112–1117.
- (20) Ren, C. E.; Hatzell, K. B.; Alhabeb, M.; Ling, Z.; Mahmoud, K. A.; Gogotsi, Y. Charge-and Size-Selective ion Sieving through Ti3C2T x MXene Membranes. *J. Phys. Chem. Lett.* **2015**, *6*, 4026–4031.
- (21) Wang, Z.; Tu, Q.; Zheng, S.; Urban, J. J.; Li, S.; Mi, B. Understanding the Aqueous Stability and Filtration Capability of MoS<sub>2</sub> Membranes. *Nano Lett.* **2017**, *17*, 7289–7298.
- (22) Joshi, R. K.; Carbone, P.; Wang, F. C.; Kravets, V. G.; Su, Y.; Grigorieva, I. V.; Wu, H. A.; Geim, A. K.; Nair, R. R. Precise and Ultrafast Molecular Sieving through Graphene Oxide Membranes. *Science* **2014**, 343, 752–754.
- (23) O'Hern, S. C.; Boutilier, M. S.; Idrobo, J.-C.; Song, Y.; Kong, J.; Laoui, T.; Atieh, M.; Karnik, R. Selective Ionic Transport through Tunable Subnanometer Pores in Single-Layer Graphene Membranes. *Nano Lett.* **2014**, *14*, 1234–1241.
- (24) Li, Y.; Zhao, W.; Weyland, M.; Yuan, S.; Xia, Y.; Liu, H.; Jian, M.; Yang, J.; Easton, C. D.; Selomulya, C.; Zhang, X. Thermally Reduced Nanoporous Graphene Oxide Membrane for Desalination. *Environ. Sci. Technol.* **2019**, *53*, 8314–8323.
- (25) Amadei, C. A.; Montessori, A.; Kadow, J. P.; Succi, S.; Vecitis, C. D. Role of Oxygen Functionalities in Graphene Oxide Architectural Laminate Subnanometer Spacing and Water Transport. *Environ. Sci. Technol.* **2017**, *51*, 4280–4288.
- (26) Abraham, J.; Vasu, K. S.; Williams, C. D.; Gopinadhan, K.; Su, Y.; Cherian, C. T.; Dix, J.; Prestat, E.; Haigh, S. J.; Grigorieva, I. V.; Carbone, P.; Geim, A. K.; Nair, R. R. Tunable Sieving of Ions Using Graphene Oxide Membranes. *Nat. Nanotechnol.* **2017**, *12*, 546–550.
- (27) Han, Y.; Xu, Z.; Gao, C. Ultrathin Graphene Nanofiltration Membrane for Water Purification. *Adv. Funct. Mater.* **2013**, 23, 3693–3700.
- (28) Kim, S.; Ozalp, E. I.; Sundar, V.; Zhu, J.-G.; Weldon, J. A. Modeling of Electrically Controlled Molecular Diffusion in a Nanofluidic Channel. *J. Appl. Phys.* **2015**, *118*, 074301.
- (29) Grahame, D. C. The Electrical Double Layer and the Theory of Electrocapillarity. *Chem. Rev.* **1947**, *41*, 441–501.

- (30) Plecis, A.; Schoch, R. B.; Renaud, P. Ionic Transport Phenomena in Nanofluidics: Experimental and Theoretical Study of the Exclusion-Enrichment Effect on a Chip. *Nano Lett.* **2005**, *5*, 1147–1155.
- (31) Nishizawa, M.; Menon, V. P.; Martin, C. R. Metal Nanotubule Membranes with Electrochemically Switchable Ion-Transport Selectivity. *Science* **1995**, *268*, 700–702.
- (32) Coleman, J. N.; Lotya, M.; O'Neill, A.; Bergin, S. D.; King, P. J.; Khan, U.; Young, K.; Gaucher, A.; De, S.; Smith, R. J.; Shvets, I. V.; Arora, S. K.; Stanton, G.; Kim, H.-Y.; Lee, K.; Kim, G. T.; Duesberg, G. S.; Hallam, T.; Boland, J. J.; Wang, J. J.; Donegan, J. F.; Grunlan, J. C.; Moriarty, G.; Shmeliov, A.; Nicholls, R. J.; Perkins, J. M.; Grieveson, E. M.; Theuwissen, K.; McComb, D. W.; Nellist, P. D.; Nicolosi, V. Two-Dimensional Nanosheets Produced by Liquid Exfoliation of Layered Materials. *Science* 2011, 331, 568–571.
- (33) Liu, Y.; He, X.; Hanlon, D.; Harvey, A.; Coleman, J. N.; Li, Y. Liquid Phase Exfoliated  $MoS_2$  Nanosheets Percolated with Carbon Nanotubes for High Volumetric/Areal Capacity Sodium-Ion Batteries. ACS Nano **2016**, 10, 8821–8828.
- (34) Tong, X.; Wang, X.; Liu, S.; Gao, H.; Xu, C.; Crittenden, J.; Chen, Y. A Freestanding Graphene Oxide Membrane for Efficiently Harvesting Salinity Gradient Power. *Carbon* **2018**, *138*, 410–418.
- (35) Zhang, Y.; Tong, X.; Zhang, B.; Zhang, C.; Zhang, H.; Chen, Y. Enhanced Permeation and Antifouling Performance of Polyvinyl Chloride (PVC) Blend Pluronic F127 Ultrafiltration Membrane by Using Salt Coagulation Bath (SCB). *J. Membr. Sci.* **2018**, 548, 32–41. (36) Lu, X.; Gabinet, U. R.; Ritt, C. L.; Feng, X.; Deshmukh, A.; Kawabata, K.; Kaneda, M.; Hashmi, S. M.; Osuji, C. O.; Elimelech, M. Relating Selectivity and Separation Performance of Lamellar Two-Dimensional Molybdenum Disulfide (MoS<sub>2</sub>) Membranes to Nanosheet Stacking Behavior. *Environ. Sci. Technol.* **2020**, *54*, 9640–9651.
- (37) Wang, J.; Zhang, L.; Xue, J.; Hu, G. Ion Diffusion Coefficient Measurements in Nanochannels at Various Concentrations. *Biomicrofluidics* **2014**, *8*, 024118.
- (38) Qu, W.; Li, D. A model for Overlapped EDL Fields. J. Colloid Interface Sci. 2000, 224, 397-407.
- (39) Hunter, R. J. Zeta Potential in Colloid Science: Principles and Applications; Academic Press, 2013; Vol. 2.
- (40) Kohonen, M. M.; Karaman, M. E.; Pashley, R. M. Debye Length in Multivalent Electrolyte Solutions. *Langmuir* **2000**, *16*, 5749–5753.
- (41) Bolt, G. H. Analysis of the Validity of the Gouy-Chapman Theory of the Electric Double Layer. *J. Colloid Sci.* **1955**, *10*, 206–218.
- (42) Achari, A.; Sahana, S.; Eswaramoorthy, M. High Performance MoS<sub>2</sub> Membranes: Effects of Thermally Driven Phase Transition on CO<sub>2</sub> Separation Efficiency. *Energy Environ. Sci.* **2016**, *9*, 1224–1228.
- (43) Ritt, C. L.; Werber, J. R.; Deshmukh, A.; Elimelech, M. Monte Carlo Simulations of Framework Defects in Layered Two-Dimensional Nanomaterial Desalination Membranes: Implications for Permeability and Selectivity. *Environ. Sci. Technol.* **2019**, *53*, 6214–6224.
- (44) Bandini, S.; Vezzani, D. Nanofiltration Modeling: the Role of Dielectric Exclusion in Membrane Characterization. *Chem. Eng. Sci.* **2003**, *58*, 3303–3326.
- (45) Bowen, W. R.; Mohammad, A. W.; Hilal, N. Characterisation of Nanofiltration Membranes for Predictive Purposes—Use of Salts, Uncharged Solutes and Atomic Force Microscopy. *J. Membr. Sci.* **1997**, *126*, 91–105.
- (46) Labban, O.; Liu, C.; Chong, T. H.; Lienhard V, J. H. Fundamentals of Pow-Pressure Nanofiltration: Membrane Characterization, Modeling, and Understanding the Multi-ionic Interactions in Water Softening. *J. Membr. Sci.* **2017**, *521*, 18–32.
- (47) Baldessari, F. Electrokinetics in Nanochannels: Part I. Electric Double Layer Overlap and Channel-to-Well Equilibrium. *J. Colloid Interface Sci.* **2008**, 325, 526–538.
- (48) Saraswat, V.; Jacobberger, R. M.; Ostrander, J. S.; Hummell, C. L.; Way, A. J.; Wang, J.; Zanni, M. T.; Arnold, M. S. Invariance of Water Permeance through Size-Differentiated Graphene Oxide Laminates. *ACS Nano* **2018**, *12*, 7855–7865.
- (49) Bowen, W. R.; Mukhtar, H. Characterisation and Prediction of Separation Performance of Nanofiltration Membranes. *J. Membr. Sci.* **1996**, *112*, 263–274.

- (50) Gopinadhan, K.; Hu, S.; Esfandiar, A.; Lozada-Hidalgo, M.; Wang, F. C.; Yang, Q.; Tyurnina, A. V.; Keerthi, A.; Radha, B.; Geim, A. K. Complete Steric Exclusion of Ions and Proton Transport through Confined Monolayer Water. *Science* **2019**, 363, 145–148.
- (51) Kim, S.; Wang, H.; Lee, Y. M. 2D Nanosheets and Their Composite Membranes for Water, Gas, and Ion Separation. *Angew. Chem.* **2019**, *131*, 17674–17689.
- (52) McCutcheon, J. R. Avoiding the Hype in Developing Commercially Viable Desalination Technologies. *Joule* **2019**, 3, 1168–1171.
- (53) Wang, Z.; Tu, Q.; Sim, A.; Yu, J.; Duan, Y.; Poon, S.; Liu, B.; Han, Q.; Urban, J. J.; Sedlak, D.; Mi, B. Superselective Removal of Lead from Water by Two-Dimensional MoS2 Nanosheets and Layer-Stacked Membranes. *Environ. Sci. Technol.* **2020**, *54*, 12602–12611.
- (54) Chen, Y.; Zhang, G.; Liu, H.; Qu, J. Confining Free Radicals in Close Vicinity to Contaminants Enables Ultrafast Fenton-like Processes in the Interspacing of MoS2 Membranes. *Angew. Chem., Int. Ed.* **2019**, *58*, 8134–8138.
- (55) Zhang, Z.; Yang, S.; Zhang, P.; Zhang, J.; Chen, G.; Feng, X. Mechanically Strong MXene/Kevlar Nanofiber Composite Membranes as High-Performance Nanofluidic Osmotic Power Generators. *Nat. Commun.* **2019**, *10*, 2920.